Journal of Alloys and Compounds 495 (2010) 162–166

Contents lists available at ScienceDirect

Journal of Alloys and Compounds

journal homepage: www.elsevier.com/locate/jallcom

Concentration effect of cerium in $(Y_{0.9-x}Gd_{0.1}Ce_x)_2SiO_5$ blue phosphor

Hiroshi Yokota[a,e,*], Masato Yoshida[b], Hiroyuki Ishibashi[a], Toyohiko Yano[c], Hajime Yamamoto[d], Shinichi Kikkawa[e]

[a] New Applied Materials R&D Center, Hitachi Chemical Co., Ltd., 1380-1 Tarasaki, Hitachinaka, Ibaraki 312-0003, Japan
[b] Advanced Materials R&D Center, Hitachi Chemical Co., Ltd., 48 Wadai, Tsukuba, Ibaraki 300-4247, Japan
[c] Research Laboratory for Nuclear Reactors, Tokyo Institute of Technology, 2-12-1 O-okayama, Meguro-ku, Tokyo 152-8550, Japan
[d] School of Bionics, Tokyo University of Technology, 1404-1 Katakura, Hachioji, Tokyo 192-0982, Japan
[e] Graduate School of Engineering, Hokkaido University, N13W8 Kita-ku, Sapporo 060-8628, Japan

ARTICLE INFO

Article history:
Received 24 June 2009
Received in revised form 15 January 2010
Accepted 20 January 2010
Available online 1 February 2010

Keywords:
Phosphors
Chemical synthesis
Crystal structure
X-ray diffraction
Optical spectroscopy

ABSTRACT

$(Y_{0.9-x}Gd_{0.1}Ce_x)_2SiO_5$ with various Ce concentration, *x*, was prepared by calcination of spray pyrolysis precursor obtained from a mixture of nitrates and TEOS under H_2/N_2 atmosphere. Cerium could be doped up to 3 at.% into the high-temperature form (X2) of Y_2SiO_5. The unit cell volume linearly expanded with the *x*-value. Its structural refinement suggested that the doped Ce^{3+} ions were almost equally distributed into two kinds of rare earth sites in the X2 phase. The PL spectra showed a peak shift toward significantly longer wavelength (red-shift) with increasing *x*-value. The PL red-shift might be caused by an energy transfer among the Ce^{3+} ions distributed in the two sites having slightly different 5d excited energy levels with different coordination numbers.

1. Introduction

Field emission displays (FEDs) have been developed as one of the new type of flat panel displays. The improvement of the phosphor materials is required to keep developments in the applications [1]. Silver-doped ZnS (ZnS:Ag) blue phosphor with high luminescence efficiency and good chromaticity has been widely used for cathode-ray tube televisions (CRTs). It gradually degrades releasing corrosive gases, H_2S and SO_x, under the FEDs electron beam irradiation [2]. The gases damage the FED tips to cause the eventual failure of the FEDs screen. Ce-doped Y_2SiO_5 (YSO:Ce) has been used as a blue phosphor for projection televisions (PTVs) because of its stability against high-current density electron beam [3,4]. This can also be an alternative for the ZnS:Ag phosphor in the FED application. The chromaticity of YSO:Ce is inferior to that of ZnS:Ag, because the emission band of YSO:Ce has a large tail extending into the red portion of the visual spectrum.

Y_2SiO_5 has two monoclinic polymorphs: low-temperature (X1) phase with the space group $P2_1/c$ (No. 14) and high-temperature (X2) phase with the space group $B2/b$ (No. 15). The X1 phase is completely transformed into the X2 phase at around 1573 K [5,6]. The usage of X2 phase in the PTVs application was realized because of its higher luminescence efficiency and less non-radiative relaxation than the X1 phase [7]. It has two different crystallographical sites, Y1 and Y2, with C_1 symmetry for rare earth ions [5]. The Y1 site has a coordination number (CN) of 7, with 5 oxide ions bonded to silicon and 2 free oxide ions. The Y2 site has a CN of 6, with 4 oxide ions bonded to silicon and 2 free oxide ions. As shown in Fig. 1, they form infinite chains of edge-sharing $O–Y_4{}^{3+}$ tetrahedra along the monoclinic *b*-axis. They interact each other through SiO_4 tetrahedra sharing their edges.

The emission of doped Ce^{3+} ions is attributed to the transition from the lowest 5d level to the $^2F_{5/2}$ and $^2F_{7/2}$ ground states having with their respective coordination environments. Suzuki et al. reported that the Ce^{3+} in Y1 and Y2 sites exhibited two independent peaks both in excitation and emission spectra at very low temperature (11 K) [8]. Additionally, Wang et al. suggested that the Ce^{3+} in Y1 site (Ce1) had lower 5d excited level than that in Y2 site (Ce2) due to the nephelauxetic effect [9,10]. The Cel showed an emission band at longer wavelength region than Ce2. Shin et al. reported that the PL spectra shifted toward longer wavelength (PL red-shift) with the increasing Ce^{3+} concentration [11]. They assumed that Ce^{3+} occupied the Y1 site more preferentially than the Y2 site with increasing Ce^{3+} concentration causing the PL red-shift. However, none of them reported any structural analysis data which could explain these luminescence properties [8–11]. It is very important to study the

* Corresponding author at: New Applied Materials R&D Center, Hitachi Chemical Co., Ltd., 1380-1 Tarasaki, Hitachinaka, Ibaraki 312-0003, Japan.
Tel.: +81 29 285 1153; fax: +81 29 285 7101.
E-mail address: hiro-yokota@hitachi-chem.co.jp (H. Yokota).

0925-8388/$ – see front matter © 2010 Elsevier B.V. All rights reserved.
doi:10.1016/j.jallcom.2010.01.112

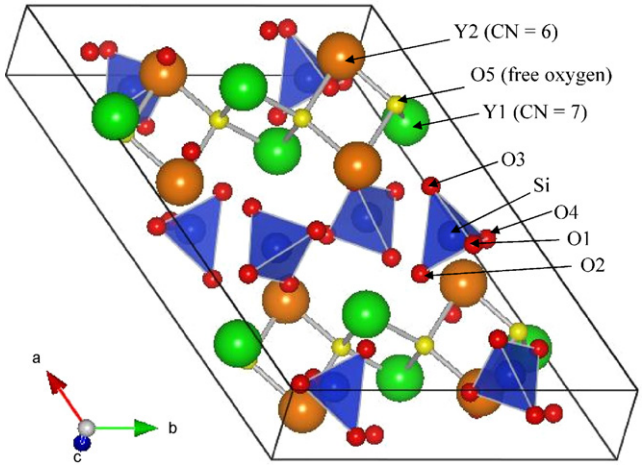

Fig. 1. Sketch of unit cell for Y_2SiO_5 high-temperature (X2) phase.

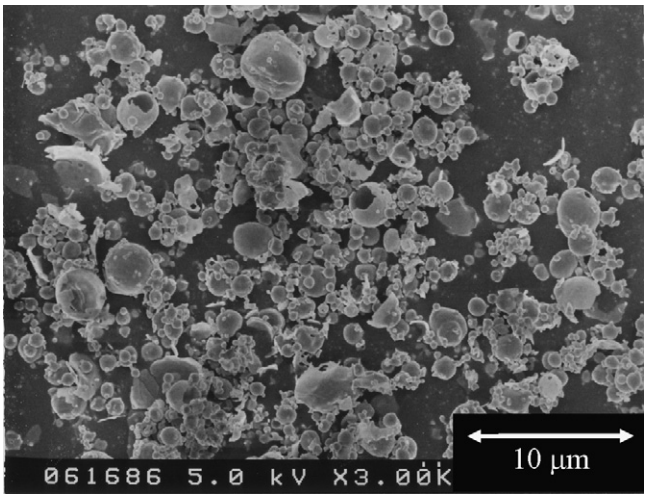

Fig. 2. SEM images of $GYSO_{0.01}$ particles.

correlation between luminescence properties and structural details such as lattice constants, site occupancy fractions, and bond length to improve a chromaticity of the YSO:Ce. However, there have been no studies concerning the correlation between structural and luminescent properties, to the best of our knowledge.

In this research, the precursors of $(Y_{0.9-x}Gd_{0.1}Ce_x)_2SiO_5$ ($GYSO_x$s) were prepared by spray pyrolysis applying a two-fluid nozzle spray generator to prepare homogeneous particles both in size and composition in large scale [12]. The Y_2SiO_5 particles containing both Gd^{3+} and Ce^{3+} have not been prepared by spray pyrolysis yet. Morphology, crystalline phases and structural details were studied on the $GYSO_x$s calcined in H_2/N_2 reductive atmosphere to avoid the oxidation of Ce^{3+}. The luminescence properties were discussed in relation to the structural details.

2. Experimental

The precursors of $GYSO_x$s were prepared by spray pyrolysis using a two-fluid nozzle spray generator (Ohkawara Kakohki, RH-2) [12]. The mixed solution of $Y(NO_3)_3$, $Gd(NO_3)_3$, $Ce(NO_3)_3$ and $Si(OC_2H_5)_4$ was sprayed into a quartz reactor (893 K) to obtain precursor particles. The reagents were purchased from Wako Chemicals, and their purity was 99.99%. Ce was doped in concentration value of x against total rare earth amount up to 20 at.%. The Gd in 10 at.% was necessary to enhance cathodoluminescence intensity in practical uses. The enhanced cathodoluminescence of Ce has been expected by the addition of Gd through energy transfer from Gd^{3+} to Ce^{3+} [13]. The excess amount of $Si(OC_2H_5)_4$ in 102.5 at.% was necessary to prevent forming Y_2O_3 impurity due to the high volatility of $Si(OC_2H_5)_4$ during the preparation [14]. These precursors were then calcinated at 1573 K under 0.5% H_2/N_2 reductive atmosphere to avoid oxidation of Ce^{3+} [11].

The pyrolysis product was observed with scanning electron microscope (SEM, Hitachi S-4500) to study the morphology and the average particle size was estimated by measuring 200 particles.

Powder X-ray diffraction (XRD) was measured by using X-ray diffractometer (Mac Science, MXP18) at 40 kV and 250 mA with monochromatized Cu Kα radiation. Data were collected in $2\theta = 10–110^\circ$ with a step scan of 0.05° (2θ) and a dwell time of 8 s at the temperature of 293 K. Cellulose resin was mixed with the samples to eliminate the preferred orientation [12]. Powdered Si (NIST 640c) was used as the external standard for the diffractometer calibration. Lattice constants and site occupancies of rare earth elements were refined by the Rietveld refinement program (RIETAN-2000) [15]. The pseudo-Voigt function was adopted as the symmetric profile shape function in the Rietveld refinement. Photoluminescence (PL) and excitation (PLE) spectra were measured with a fluorescence spectrometer (Hitachi, F-4500).

3. Results and discussion

3.1. Morphology and crystal structure

Well-dispersed spherical particles were obtained in $GYSO_{0.01}$ as shown in Fig. 2. A mean particle size of 2.5 μm and the spherical shape were observed independently on the Ce doping level x in $GYSO_x$s.

In the case for $GYSO_{0.01}$, almost pure high-temperature (X2) phase of Y_2SiO_5 (JCPDS # 21-1458) was obtained with a very small amount of apatite $Y_{4.67}(SiO_4)_3O$ (JCPDS # 30-1457) impurity as depicted in Fig. 3(a). The similar XRD patterns were also observed in the case for $GYSO_0$, $GYSO_{0.03}$, $GYSO_{0.04}$, and $GYSO_{0.05}$. On the other hand, the low-temperature (X1) phase of Y_2SiO_5 (JCPDS # 21-1456) appeared above $x = 0.10$, and became significant at $x = 0.20$ as depicted Fig. 3(b). The X1 phase formation can be attributed to the reported preference of Ce^{3+} with remarkably larger ionic size in higher coordination number of 9 and 7 in the X1 phase in rare earth sites rather than Gd^{3+} [5,9].

The $GYSO_x$ products in $x = 0–0.05$ were mainly the X2 phase, and the monoclinic lattice parameters were refined. The refinements were well converged on the product without cerium. The structural parameters of $GYSO_0$ are summarized in Table 1. The reliability fac-

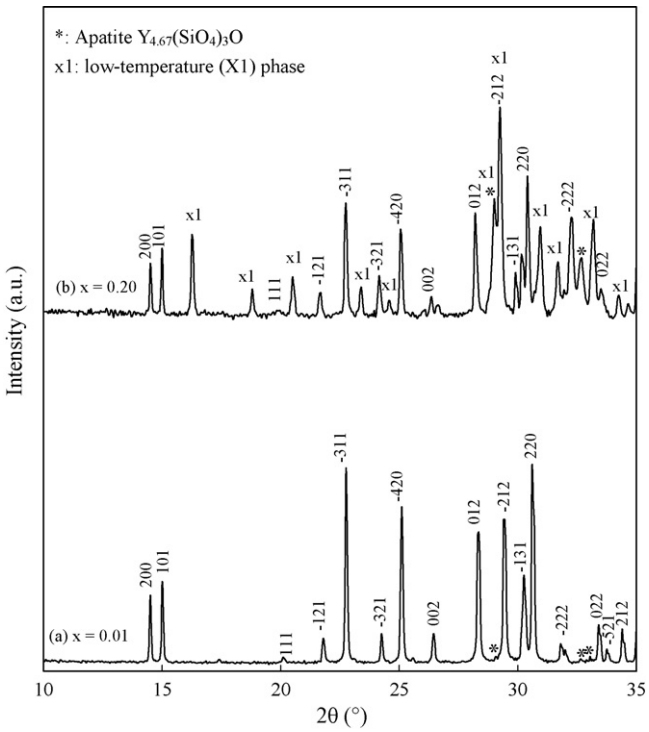

Fig. 3. XRD patterns of $GYSO_x$s (x denotes Ce doping level): (a) $GYSO_{0.01}$ and (b) $GYSO_{0.20}$.

Table 1
Refined structural parameters of $GYSO_0$ obtained from the Rietveld refinement[a].

Atom	Position	x	y	z	g[b]	B (10^{-2} nm^2)[c]
Y1	8f	0.2883(3)	−0.0348(5)	0.9968(5)	0.901(3)	0.67(8)
Gd1	8f	0.2883(3)	−0.0348(5)	0.9968(5)	0.099(3)	0.67(8)
Y2	8f	0.1083(3)	−0.3352(5)	0.6283(5)	0.899(3)	0.79(9)
Gd2	8f	0.1083(3)	−0.3352(5)	0.6283(5)	0.101(3)	0.79(9)
O1	8f	0.1265(13)	−0.3096(21)	−0.0318(24)	1.0	0.59
O2	8f	0.1524(15)	−0.1543(24)	0.2474(26)	1.0	0.60
O3	8f	0.9524(16)	−0.3288(22)	0.0952(27)	1.0	0.41
O4	8f	0.0504(14)	−0.4276(23)	0.3092(26)	1.0	0.89
O5	8f	0.2673(15)	−0.1008(21)	0.6400(25)	1.0	0.42
Si	8f	0.0692(9)	−0.3060(13)	0.1620(17)	1.0	0.10(4)

[a] Space group: $B2/b$ (No. 15). The analysis reliabilities R_I = 3.6%, and the goodness-of-fit indicators $S(R_{wp}/R_e)$ = 1.9.
[b] Occupation factor.
[c] Isotropic atomic displacement factor. The value for O1–O5 was fixed the data for the single crystal refinement [5].

tors R_I and the goodness-of-fit indicators $S(R_{wp}/R_e)$ for the refined products were 3.4–5.3%, and 1.6–2.5, respectively. Its lattice constants a, b, c, V, and the most of the Y–O distances were slightly larger than those reported for Y_2SiO_5 without cerium and gadolinium as represented in Table 2 [16], due to the Gd^{3+} doping with larger ionic radius than Y^{3+}. The lattice constants a and c increased up to x = 0.03, and became constant because of the solubility limit of Ce^{3+} in a range of x = 0.03 to 0.05 as depicted in Fig. 4. The unit cell volume also expanded with the value of x up to x = 0.03. Lattice constant b expanded with the cerium amount, but there was no tendency on γ-value. As shown in Fig. 1, the rare earth sites (Y1 and Y2) form infinite chains of edge-sharing O–Y_4^{3+} tetrahedra running along the monoclinic b-axis together with free oxide ions. Consequently, it was found that $GYSO_x$s crystal lattice tends to expand preferentially along with b-axis in twice with the value of x. Additionally, the unit cell volume data also suggest that cerium could be doped up to x = 0.03 into the X2 phase of Y_2SiO_5.

Both Gd^{3+} and Ce^{3+} ions were doped together into Y_2SiO_5. Their occupancy fractions in Y1 and Y2 sites were refined assuming that the doped Gd^{3+} and Ce^{3+} independently occupied these sites, as summarized in Table 3. The Ce and Gd occupancies were almost the same between Y1 and Y2 sites and the values were also the same with the total amount of the doped ones. Consequently, the

Table 2
Bond distances and unit cell parameters of the Y_2SiO_5 (refs) and $GYSO_0$.

	$GYSO_0$	Y_2SiO_5[a]
Unit cell parameters		
a (nm)	1.4410(1)	1.4371(3)
b (nm)	1.0433(1)	1.0388(3)
c (nm)	0.6731(1)	0.6710(4)
γ (°)	122.18(1)	122.17(4)
V (nm^3)	0.856(1)	0.848(1)
Main bond distances (10^{-1} nm)		
Y1–O1	2.51(1)	2.374
Y1–O1	2.56(1)	2.604
Y1–O2	2.37(2)	2.299
Y1–O2	2.41(2)	2.317
Y1–O3	2.28(1)	2.319
Y1–O5	2.17(1)	2.199
Y1–O5	2.47(2)	2.373
Y2–O1	2.30(2)	2.283
Y2–O3	2.31(1)	2.275
Y2–O4	2.32(2)	2.280
Y2–O4	2.35(2)	2.287
Y2–O5	2.22(2)	2.203
Y2–O5	2.29(2)	2.279
Si–O1	1.56(2)	1.628
Si–O2	1.50(2)	1.636
Si–O3	1.63(3)	1.602
Si–O4	1.52(2)	1.605

[a] Ref. [16].

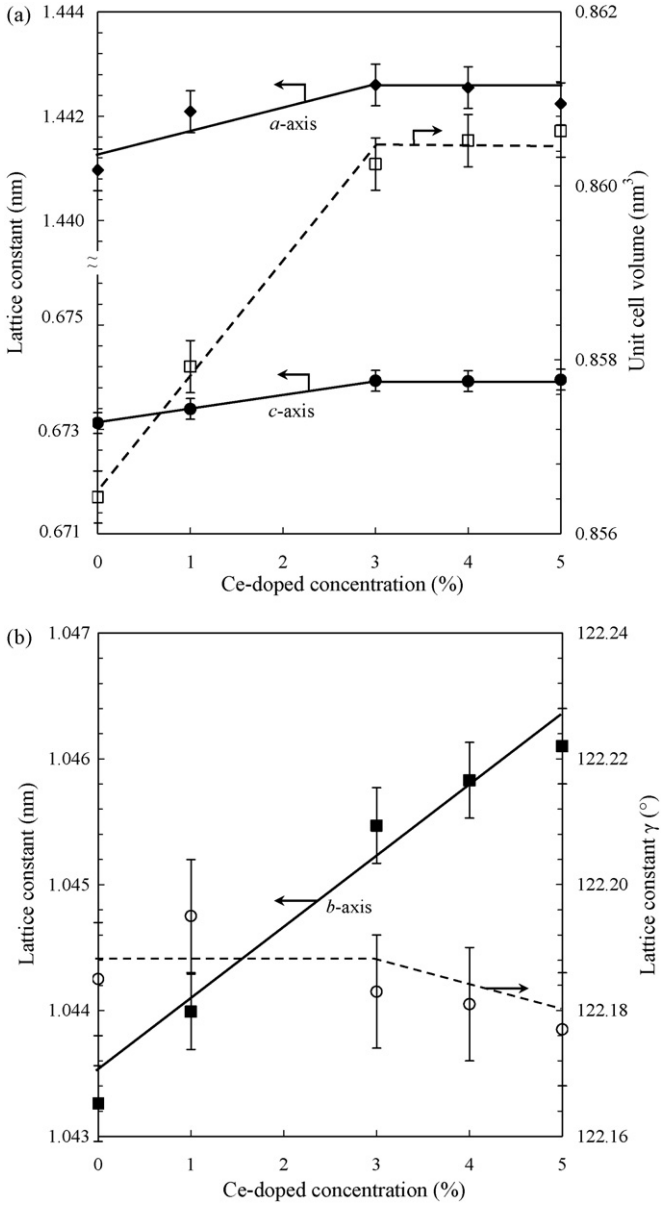

Fig. 4. Lattice constants of $GYSO_x$s (from x = 0 to 0.05) refined by XRD-Rietveld refinement: (a) lattice constants a, c, and unit cell volume, and (b) lattice constants b and γ.

Table 3
Site occupancy fractions of Gd and Ce for $GYSO_x$s. Gd1 and Ce1 denote site occupancy fractions substituted of Y1 site, Gd2 and Ce2 denote that of Y2 site.

Site occupancy fraction	Y1	Gd1	Ce1	Y2	Gd2	Ce2
H-$GYSO_0$	0.901(3)	0.099(3)	–	0.899(3)	0.101(3)	–
H-$GYSO_{0.01}$	0.886(3)	0.104(3)	0.010(3)	0.894(3)	0.096(3)	0.010(3)
H-$GYSO_{0.03}$	0.858(3)	0.112(3)	0.030(3)	0.882(3)	0.088(3)	0.030(3)

Ce^{3+} occupied both the Y1 and Y2 sites in almost the equal fraction as in the cases of Y^{3+} and Gd^{3+}.

3.2. Luminescence properties

Both $GYSO_{0.01}$ and $GYSO_{0.03}$ showed the excitation maxima at around 360 nm with shoulders at 310 nm as shown in Fig. 5. The spectra were very similar to each other. PL spectrum of $GYSO_{0.01}$ showed a broad band with maximum intensities at around 424 nm with a shoulder at around 410 nm and a tailing to longer wavelength. $GYSO_{0.03}$ showed a significant red-shift with maximum intensities at around 472 nm in the similar broad band. In addition, a full width at half maximum of the asymmetric luminescence peak for $GYSO_{0.03}$ was broader than for $GYSO_{0.01}$.

Shin et al. reported that the PL spectra shifted toward longer wavelength with increasing Ce^{3+} concentration. The shift toward longer wavelength (red-shift) was explained by the Ce^{3+} preferential occupation of the Y1 site than the Y2 site in the increased Ce^{3+} concentration. However, structural analysis data were never shown in their report [11]. The present result indicated that the preferential site occupation was not observed for Ce^{3+}. The present PL red-shift with *x*-value was not caused by the preferential Y1 or Y2 sites occupation of Ce^{3+}. The Ce^{3+} ions in two different rare earth sites transfer the energy in the respective 5d excited level to each other.

The theory of energy transfer has been elucidated by Dexter [17,18]. The energy transfer occurs in electric dipole in the case of Ce^{3+}. Its transfer probability, P_{DA}, from one (donor) to the other (accepter) is given as follows:

$$P_{DA} = \frac{3c^4\hbar^4}{4\pi n^4 R^6} \times \frac{\sigma_A}{\tau_A} \times \int \frac{f_D(E)F_A(E)}{E^4} dE \quad (1)$$

Here, R is the separation between the donor (D) and the accepter (A), n is the refractive index of the crystal, σ_A is the absorption cross-section of A, and τ_A is the radiative lifetime of A. The Ce^{3+} in the Y1 site (Ce1) had lower 5d excited level than that in the Y2 site (Ce2) due to the nephelauxetic effect in their respective coordination numbers of 7 and 6 in the present case [10]. The Cel and Ce2 can be regarded as the accepter and the donor, respectively. $f_D(E)$ and $F_A(E)$ represent the shape of the D emission and A absorption (excitation) spectra, respectively. They have been normalized as $\int f(E)dE = 1$ and $\int F(E)dE = 1$. Therefore, the integrals in Eq. (1) corresponding to the overlapping of these spectra are necessary for energy transfers to occur. Both the PLE (λ_{em} = 472 nm) and PL (λ_{ex} = 356 nm) spectra (Fig. 5) overlap each other at the wavelength around 380 nm to satisfy the integrals in Eq. (1). In addition, the term R^{-6} in Eq. (1) means that the energy transfer probability increases significantly with decreasing D–A distances, *i.e.*, the increase of cerium concentration. Furthermore, the Y1 and Y2 sites in $GYSO_x$s are comparatively close to each other as shown in Table 4, for the energy transfer between them to occur easily. For these reason, energy transfers (Ce2 → Ce1) between the two independent Ce^{3+} ions in the Y1 and Y2 sites increase with the *x*-value, to cause PL red-shift. The similar phenomena have been reported on Eu^{2+}- and Mn^{2+}-doped phosphors, in their f–d and d–d type transitions, respectively [19–22].

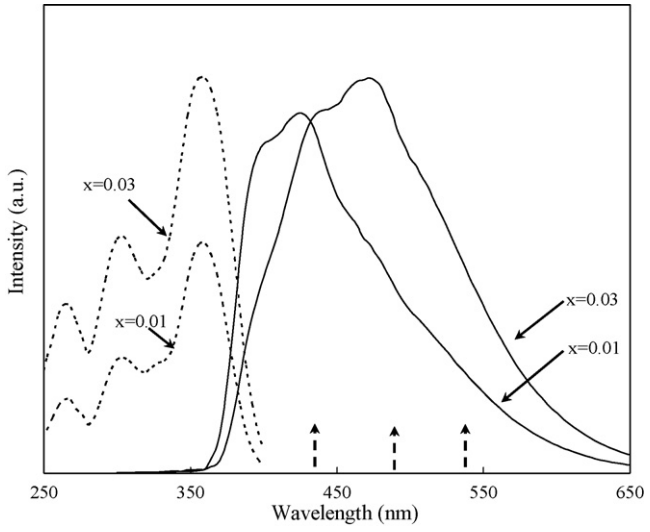

Fig. 5. PL (λ_{ex} = 356 nm) and PLE (λ_{em} = 472 nm) spectra of $GYSO_{0.01}$ and $GYSO_{0.03}$.

Table 4
Yttrium–yttrium distances in $GYSO_0$ according to the refined structural data[a].

Neighbor number	1	2	3	4	5
Type of neighbor	Y1–Y2	Y2–Y2	Y1–Y2	Y1–Y1	Y1–Y2
Distance (10^{-1} nm)	3.42(1)	3.48(1)	3.52(1)	3.69(1)	3.75(1)

[a] $GYSO_{0.01}$ and $GYSO_{0.03}$ also had the same type of neighbor as $GYSO_0$.

4. Conclusions

The effect of the doped Ce^{3+} ions was studied on structural and luminescent properties of $(Y_{0.9-x}Gd_{0.1}Ce_x)_2SiO_5$. The refined site occupancy indicated that Ce^{3+} ions distributed in both Y1 with CN = 7 and Y2 with CN = 6 sites in GYSOs almost equally, regardless of *x*-value. On the other hand, PL spectra were shifted toward a longer wavelength with increasing cerium amount. The PL red-shift with *x*-value might be caused by the energy transfer between two independent Ce^{3+} ions in Y1 and Y2 sites.

References

[1] P.J. Marsh, J. Silver, A. Vecht, A. Newport, J. Lumin. 97 (2002) 229–236.
[2] E.J. Bosze, G.A. Hirata, L.E. Shea-Rohwer, J. McLittrick, J. Lumin. 104 (2003) 47–54.
[3] P.J. Born, D.S. Robertson, P.C. Smith, J. Mater. Sci. Lett. 4 (1985) 497–501.
[4] S. Erdei, R. Roy, G. Harshe, H. Juwhari, D. Agrawal, F.W. Ainger, W.B. White, Mater. Res. Bull. 30 (1995) 745–753.
[5] J. Felsche, Structure and Bonding, vol. 13, Springer, Berlin, 1973, pp. 99–97.
[6] J. Wang, S. Tian, G. Li, F. Liao, X. Jing, Mater. Res. Bull. 36 (2001) 1855–1861.
[7] J. Lin, Q. Su, S. Wang, H. Zhang, J. Mater. Chem. 6 (1996) 265–269.
[8] H. Suzuki, T.A. Tombrello, C.L. Melcher, J.S. Schweitzer, Nucl. Instrum. Methods A 320 (1992) 263–272.
[9] J. Wang, S. Tian, G. Li, F. Liao, X. Jing, J. Electrochem. Soc. 148 (2001) H61–H66.
[10] H. Jiao, F. Liao, S. Tian, X. Jing, J. Electrochem. Soc. 151 (2004) J39–J42.
[11] S.H. Shin, D.Y. Jeon, K.S. Sun, Jpn. J. Appl. Phys. 40 (2001) 4715–4719.
[12] H. Yokota, M. Yoshida, Y. Yagi, H. Ishibashi, T. Yano, H. Yamamoto, Jpn. J. Appl. Phys. 47 (2008) 167–172.
[13] J. Shmulovich, G.W. Berkstresser, C.D. Brandle, A. Valentino, J. Electrochem. Soc. 135 (1988) 3141–3151.
[14] Y.C. Kang, I.W. Lenggoro, S.B. Park, K. Okuyama, J. Solid State Chem. 146 (1999) 168–175.

[15] F. Izumi, T. Ikeda, Mater. Sci. Forum 321–324 (2000) 198–203.
[16] D. Chiriu, N. Faedda, A.G. Lehmann, P.C. Ricci, Phys. Rev. B 76 (2007), 054112(1)–054112(8).
[17] D.L. Dexter, J. Chem. Phys. 21 (1953) 836–850.
[18] W.M. Yen, S. Shionoya, H. Yamamoto, Fundamentals of Phosphors, CRC Press, New York, 2006, p. 89–100.
[19] C.R. Ronda, T. Amrein, J. Lumin. 69 (1996) 245–248.
[20] P. Thiyagarajan, M. Kottaisamy, M.S.R. Rao, J. Phys. D: Appl. Phys. 39 (2006) 2701–2706.
[21] M.S. Kwon, C.J. Kim, H.L. Park, T.W. Kim, H.S. Lee, J. Mater. Sci. 40 (2005) 4089–4091.
[22] G. Blasse, J. Solid State Chem. 62 (1986) 207–211.